Single-molecule compaction of megabase-long chromatin molecules by multivalent cations

Anatoly Zinchenko[1],[2],*,†, Nikolay V. Berezhnoy[2],†, Sai Wang[2], William M. Rosencrans[3], Nikolay Korolev[2], Johan R.C. van der Maarel[4] and Lars Nordenskiöld[2],*

[1]Graduate School of Environmental Studies, Nagoya University, Furo-cho, Chikusa-ku, Nagoya, 464-8601, Japan, [2]School of Biological Sciences, Nanyang Technological University, 60 Nanyang Drive, 637551 Singapore, [3]Department of Physics and Astronomy, Colgate University, Hamilton, NY 13346, USA and [4]Department of Physics, National University of Singapore, 117542 Singapore

ABSTRACT

To gain insight into the conformational properties and compaction of megabase-long chromatin molecules, we reconstituted chromatin from T4 phage DNA (165 kb) and recombinant human histone octamers (HO). The unimolecular compaction, induced by divalent Mg^{2+} or tetravalent spermine^{4+} cations, studied by single-molecule fluorescence microscopy (FM) and dynamic light scattering (DLS) techniques, resulted in the formation of 250–400 nm chromatin condensates. The compaction on this scale of DNA size is comparable to that of chromatin topologically associated domains (TAD) *in vivo*. Variation of HO loading revealed a number of unique features related to the efficiency of chromatin compaction by multivalent cations, the mechanism of compaction, and the character of partly compact chromatin structures. The observations may be relevant for how DNA accessibility in chromatin is maintained. Compaction of saturated chromatin, in turn, is accompanied by an intrachain segregation at the level of single chromatin molecules, suggesting an intriguing scenario of selective activation/deactivation of DNA as a result of chromatin fiber heterogeneity due to the nucleosome positioning. We suggest that this chromatin, reconstituted on megabase-long DNA because of its large size, is a useful model of eukaryotic chromatin.

INTRODUCTION

DNA compaction within the confined space of the eukaryotic cell nucleus in the form of chromosomes is a hierarchical process of outstanding biological significance for storage of genomic DNA molecules, which are several hundreds of megabases long. A well-defined nucleosome core particle (NCP) is formed by wrapping of about 147 bp DNA in 1.75 turns around the histone octamer (HO) (Figure 1A) (1,2). The HO consists of two copies each of the core histones H2A, H2B, H3 and H4. Figure 1A illustrates that the NCP is a polyanion-polycation complex with a net negative charge of about $-146e$, resulting from the negatively charged central particle (with $-294e$ from DNA and $+52e$ from the globular part of the HO). Protruding out from the HO core are ten flexible and positively charged histone tails with a net charge $+96e$, eight of which are N-terminal tails and two C-terminal H2A tails. The NCPs are wedge shaped particles of 11 nm diameter and 6 nm height. The NCPs connected by linker DNA of variable length (20–70 bp) in extended conformation are known as 'beads on a string' 10 nm fiber, where the nucleosomes are the fundamental repeating units of chromatin. Nucleosome formation results in diminishing of the effective DNA length. The packing of the 10 nm fiber requires charge neutralization and internucleosomal contacts. Nucleosomes represent the elementary functional assembly for selective access to the DNA genetic information via compaction-decompaction that is mediated by a variety of proteins including linker histones, polycations, posttranslational modifications (3), and histone variants (4).

Physico-chemical studies of the anionic chromatin of native and recombinant origin demonstrated its polyelectrolyte behavior in the presence of multivalent cations that induce condensation and re-dissolution (5,6). Most of the

*To whom correspondence should be addressed. Tel: +65 6790 3737; Fax:+65 6896 8032; Email: LarsNor@ntu.edu.sg
Correspondence may also be addressed to Anatoly Zinchenko. Email: zinchenko@urban.env.nagoya-u.ac.jp
†These authors contributed equally to this work as first authors.
Present address: Nikolay V. Berezhnoy, Singapore Center for Environmental Life Sciences Engineering, Nanyang Technological University, 60 Nanyang Drive, 637551 Singapore.
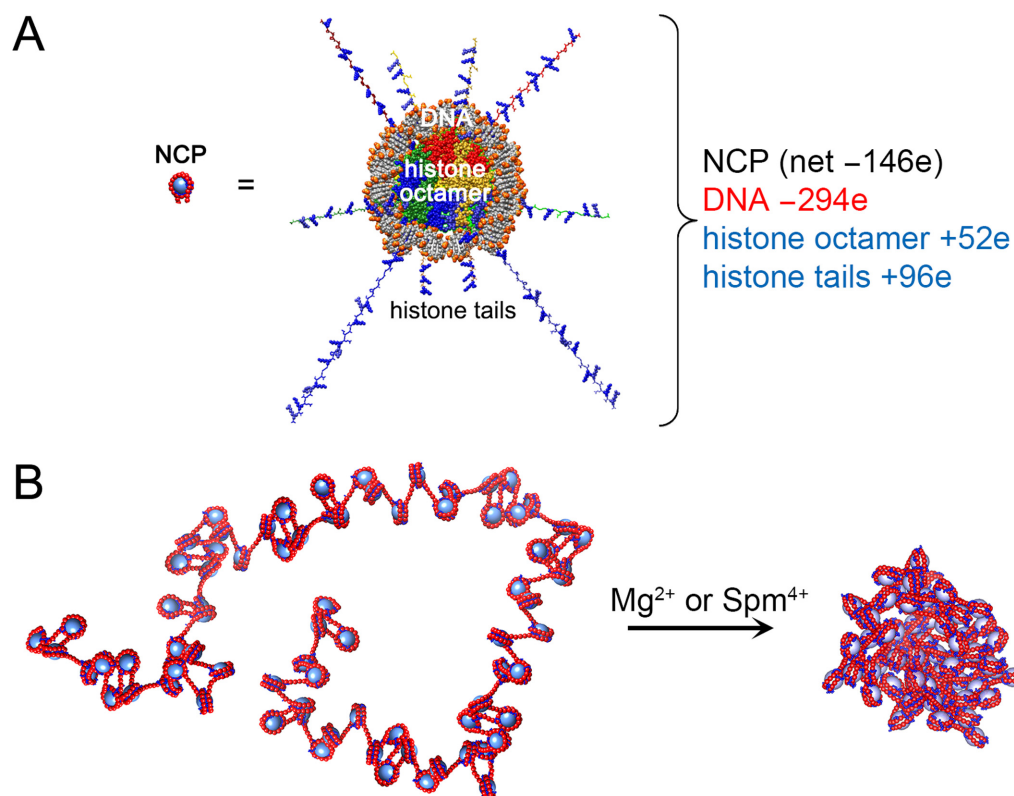
Figure 1. Experimental system. (**A**) Structure of the nucleosome core particle (NCP). Chromatin reconstituted in this study contains no linker histones. (**B**) Schematic representation of chromatin fiber comprising a large number of nucleosome core particles and a coil to globule conformational transition upon addition of divalent (Mg^{2+}) or tetravalent (spermine, SPM^{4+}) cations.

studies examined condensation/aggregation of chromatin predominantly at the level of nucleosomes or short nucleosome arrays. Particularly, *in vitro* reconstituted nucleosome arrays using DNA array templates based on the Widom '601' high affinity nucleosome positioning sequence, and with less than a hundred HOs bound per DNA molecule were successfully studied to address the structure of the 30 nm chromatin fiber, chromatin compaction and aggregation (7–9). Other studies particularly focused on the important role of structural recognition of certain DNA sequences by histone proteins, their positioning, and gene regulation (10).

Studies of eukaryotic genomes by chromatin conformation capture-based methods (11) and *in situ* fluorescence techniques (12) suggest that interphase chromatin is organized into cell-type specific chromosome territories (13), occupied by individual chromosomes. Each chromosome territory consists of independent and dynamic topologically associated domains (TAD) (14,15). In human nuclei, TADs are around one megabase-long chromosomal fragments of around 300 or 240 nm in radius, representing euchromatin or heterochromatin regions, respectively (16). At present, studies of long DNA molecules reconstituted with several hundred HOs forming megabase-long chromatin are scant (17,18), and further *in vitro* physico-chemical studies are important to improve our understanding of chromatin organization in nuclei of living cells.

In vitro studies on model systems showed that the DNA compaction mechanism and the accompanied changes of DNA biological activity differ dramatically between short and long (>10 kbp) DNAs (19). For example, long-chain DNA exhibits a first order phase transition at the level of individual molecules upon addition of multivalent cations (20), while the compaction of short DNA molecules exhibits a gradual aggregation of DNA into a water-insoluble complex. Consequently, the discrete conformational transition of long DNA abruptly 'switches off' the DNA transcriptional activity at the point of the compaction, whereas the genetic activity of short DNA correlates with the degree of DNA aggregation (21). To gain a deeper insight into the problem of long DNA chain compaction in the presence of nucleosome-forming HOs, studies on DNA compaction and transcription by histone-mimicking cationic dendrimers (22) and cationic nanoparticles of several sizes (23,24), have been performed. Compaction of long DNA by natural HOs and the behavior of such a biologically relevant system deserves a thorough investigation. The possibility of gene regulation by solely controlling the DNA conformational state (folded of collapsed) remains an open question (25).

The present work was motivated by the importance of DNA length in the DNA compaction process and is focused on unimolecular folding of megabase-long reconstituted chromatin. We report the conformational behavior and compaction of chromatin reconstituted from giant T4 phage DNA (165.6 kb, contour length ca. 60 μm) and recombinant human HOs as a function of the degree of

loading of DNA by HOs and of the nature of polycation added (Mg^{2+} and spermine^{4+}), using direct single-molecule DNA visualization in bulk solution by fluorescence microscopy and measurements with the dynamic light scattering method. The reconstituted chromatin in this study, characterized by MNase assay and negative stain TEM, under low salt conditions was shown to form micrometer-sized beads-on-a-string chromatin with a somewhat heterogeneous distribution of nucleosomes on the DNA. The size is close to that of TADs in cell nuclei and this study is the first attempt to address compaction for *in vitro* reconstituted chromatin fibers of size similar to the TADs of eukaryotic chromatin *in vivo*. This chromatin reconstituted on long DNA without preferential nucleosome positioning, should serve as a reasonable model of human eukaryotic chromatin because a common characteristic of chromatin *in vivo* is that the majority of the nucleosomes in the human genome are not preferentially positioned (26). Nucleosome arrays based on DNA templates with high affinity positioning elements on the other hand, are regularly positioned and are size-limited due to their repetitive design.

MATERIALS AND METHODS

The linear T4GT7 DNA was purchased from Nippon Gene Co. Ltd. (Japan). The molar concentration of DNA shows the concentration of DNA phosphate groups (i.e. DNA monomer units, nucleotides). The fluorescent dye YOYO-1 (1,1′-(4,4,7,7-tetramethyl-4,7-diazaundecamethylene)-bis-4-[3-methyl-2,3-dihydro-(benzo-1,3-oxazole)-2-methylidene]-quinolinium tetraiodide) was provided by Molecular Probes (Invitrogen, Japan). NaCl, $MgCl_2$, and spermine tetrahydrochloride were purchased from Nacalai Tesque Inc. (Kyoto, Japan). Deionized water (Milli-Q, Millipore) was used for samples preparation. TE-KCl buffer (10 mM Tris–HCl, 1 mM EDTA, pH = 7.8) containing 10 mM of KCl was used in all experiments, except for transmission electron microscopy where Tris was replaced by HEPES.

Preparation of recombinant chromatin

The coding sequences of recombinant human core histones H2A, H2B and H3.1 were cloned in the pET21a vector, and the H4 histone coding sequence in the pET3a vector. Each core histone was individually expressed in the *Escherichia coli* BL21(DE3)-pLysS strain, purified from inclusion bodies using size-exclusion and cation-exchange chromatography following the established protocol (27).

The HOs were refolded from the equimolar mixture of core histones, purified using size-exclusion chromatography following established protocol (27) and assessed on SDS-PAGE (Supplementary Figure S1).

Reconstitution of the T4 DNA with HO was performed using the salt dialysis approach (17,18,28,29). DNA complexes with HO at different degrees of loading were reconstituted by adding 11%, 16%, 23%, 32%, 45%, 66%, 90%, 113%, 128%, 131%, 163% and 200% of HO, calculated based on a ratio of one HO per 200 bp of DNA. For example, 100% loading corresponds to 828 HO molecules per DNA molecule. A typical chromatin reconstitution mixture

of 50 μl contained DNA at 0.1 μg/μl, 2 M KCl, 20 mM Tris pH 7.5, 1 mM EDTA pH 8 and 1 mM DTT. The reconstitution mixture was loaded into a Slide-A-Lyzer MINI dialysis unit (3500 MWCO, Thermo Scientific) and dialyzed at room temperature at constant mixing in 200 ml of the initial buffer containing 2 M KCl, 20 mM Tris, 1 mM EDTA and 1 mM DTT.

UV–Vis spectroscopy

DNA concentration was measured in samples after chromatin reconstitution with a NanoDrop 2000 UV–Vis Spectrophotometer (Thermo Scientific, NanoDrop Products, Wilmington, Delaware, USA) at 25°C.

Dynamic light scattering (DLS)

Dynamic light scattering (DLS) experiments were conducted using a Zetasizer Nano ZS (Malvern Instruments Ltd, Worcestershire, UK) at 25°C. A laser beam was passed through a 1 ml quartz cell containing 0.66 ng/μl (2 μM) T4 DNA in buffer with an appropriate amount of condensing agent (spermine or $MgCl_2$), and the scattered light was measured at a 173° angle to the incident beam. The hydrodynamic size of compact DNA condensates was obtained as a *Z*-average value (cumulus mean).

Fluorescence microscopy (FM)

Sample solutions for single molecule observations were prepared by successive mixing of water, concentrated solution of chromatin at the final DNA concentration of 0.066 ng/μl (0.2 μM), fluorescent dye YOYO (20 nM), and a solution of the multivalent cation as the compaction agent. Solution components were gently mixed after addition of a new component and the final samples were incubated for 1 hour at ambient temperature prior to observations. FM observations were performed using an Eclipse TE2000-U (Nikon, Japan) microscope equipped with 100 × oil-immersion lens. Fluorescent images were recorded and analyzed using an EB-CCD camera and an Argus 10 image processor (Hamamatsu Photonics, Japan).

Transmission electron microscopy (TEM)

Square mesh copper grids (Maxtaform 400, EMS) were coated by 10 nm carbon layer using Leica EM ACE600. Chromatin at 5 ng/μl was fixed by 0.01% glutaraldehyde on ice for 10 min, loaded onto the freshly glow-discharged grids, and negatively stained by 2% uranyl acetate. The grids were air-dried at room temperature and observed with a Tecnai T12 microscope equipped with Eagle 4K CCD camera (FEI).

Atomic force microscope (AFM)

A 5 μl droplet of reconstituted T4 chromatin at 32 ng/μl was spotted onto a silica surface. After 10 min to allow for DNA adsorption onto the surface, the specimens were developed by flushing them with ultra-pure water followed by drying in a stream of N_2 gas. Atomic force imaging was

done with a Bruker Dimension Icon microscope (Billerica, MA, USA) at room temperature in air. Images were acquired in the tapping mode with silicon (Si) cantilevers (spring constant of 19–55 N/m) and operated below their resonance frequency (typically 270–370 kHz). The images were flattened, and the contrast and brightness were adjusted for optimal viewing conditions.

Pulsed-field gel electrophoresis

The electrophoretic mobility shift of T4 DNA reconstituted with histone octamers was assessed using pulsed-field gel electrophoresis using CHEF-DR II system (BioRad). Equivalent of 0.2 μg DNA with 5% sucrose were loaded into 0.7% Megabase agarose (BioRad) in 0.2× Tris–borate buffer and separated at 3 V/cm with switch gradient from 60 to 120 s over 24 h at 14°C.

Micrococcal nuclease digestion of reconstituted chromatin

Chromatin was digested by Micrococcal Nuclease (MNase) (New England Biolabs) following established procedure with modifications (30). 16 μg of DNA were digested for 10 min at room temperature following manufacturer's guidelines using 0.05 U/μl and 0.3 U/μl of MNase. Digestion was stopped by addition of EDTA to 100 mM final concentration. After the addition of 25 μg of Proteinase K (Thermofisher Scientific), the solution was incubated at 50°C for 30 min. The DNA was purified on a Wizard SV Gel and PCR clean-up system (Promega) and run on 10% polyacrylamide gel electrophoresis at 100 V at room temperature.

Nucleosome occupancy analysis of T4 DNA sequence

The sequence analysis was performed using an algorithm available online (31). The sequence of T4GT7 DNA (GenBank: KJ477686.1) was divided into five fragments with overlapping regions of 5250 bp. Default parameters for *in vitro* reconstitution were used: amplitude 0.2; period 10.1 bp; window 74 bp; and potential −1.0 kT. Regions of DNA sequences with values of nucleosome occupancy higher than 0 indicate areas of high nucleosome affinity with nucleosome positioning effect.

RESULTS

Validation of nucleosome formation on T4 DNA in *in vitro* reconstitution at different degrees of loading with histone octamer

In contrast to a vast number of studies of nucleosome arrays that were performed on relatively short DNAs, T4 DNA used in the present work contains 165,660 bp that are sufficient to form ~900 nucleosomes on the DNA chain. A series of DNA complexes with HO in the loading range of 11–200% were reconstituted using the salt dialysis approach, based on a ratio of one histone octamer per 200 bp of DNA. Variation of DNA loading with HOs allows for a sampling of different average nucleosome repeat lengths (NRL), which previously was demonstrated to affect the structure of chromatin fibers on the 10–30 nm level (9,32).
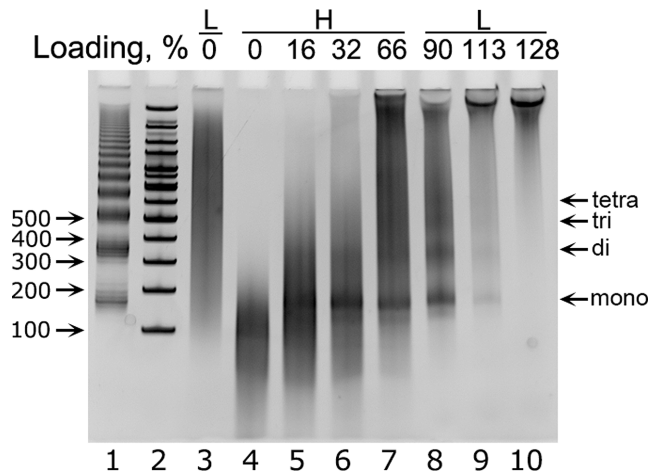

Figure 2. *In vitro* reconstituted T4 DNA with HO at different degree of loading was digested by micrococcal nuclease (lanes 3–10). In lanes 3 and 8–10, low concentrations (0.05 U/μl) of MNase were used (L); in lanes 4–7, high concentrations of MNase (0.3 U/μl) were used (H). T4 DNA in the absence of HO shows digestion dependence on MNase concentration (lanes 3 and 4). 100 bp marker DNA (lane 2) allows to estimate that DNA in multiples of around 150 bp is protected from MNase in the presence of HO at 16–113% loading degrees (lanes 5–9). T4 DNA at higher degrees of HO loading is protected from MNase digestion (lane 10). Nucleosome array with 601 nucleosome positioning sequence of 36 nucleosomes with 177 bp nucleosome repeat length digested by MNase (lane 1) produces nucleosome ladder upon incomplete digestion and was used as a positive control.

A gradual decrease in the electrophoretic mobility of the reconstituted chromatin was observed using pulsed-field gel electrophoresis (PFGE) indicating the increased binding of HO to DNA with higher HO loading (Supplementary Figure S2).

Micrococcal nuclease that digests DNA not bound by proteins (33) was used to demonstrate the formation of nucleosomes. Distinct DNA protection band pattern of around 150 bp after MNase digestion results from DNA wrapped around the HO (Figure 2). MNase digestion is highly sensitive to the conditions of the reaction, such as the amounts and molecular weight of DNA, amount of MNase, duration and temperature. Two concentrations of MNase that allow better characterization of reconstituted chromatin at different loading degrees of HO were used. Using high concentration of MNase results in sufficient digestion of DNA and visualization of the 150 bp DNA protection pattern at both low and high loading degrees of HO in the range of 16–131% (lanes 4–7 on Figure 2, see also Supplementary Figure S3A). At low concentration of MNase, partial digestion of DNA and chromatin at low degrees of HO loading results in smeared higher molecular weight DNA bands (Supplementary Figure S3B). At HO loading degrees of 90% and 113% around the saturation, partial digestion results in a ladder pattern in multiples of 150 bp, indicating the release of not only mononucleosomes, but also di-, tri-, and tetranucleosomes (lanes 8 and 9 on Figure 2, see also Supplementary Figure S3B). Because the T4 DNA is not a positioning sequence, unlike the control nucleosome array with the 601 sequence of 36 nucleosomes with 177 bp NRL (Figure 2, lane 1), the difference in MNase digestion is not unexpected. Partial MNase digestion, accompanied

by DNA smears that allow detection of tetranucleosomes as the largest product that can be resolved, indicates a heterogeneous distribution of the NRL in T4 chromatin (see below on TEM results). This is in agreement with observations for MNase digestion of nucleosome arrays reconstituted on telomeric DNA formed by repetitive TTAGGG repeats that lack positioning elements (34). At higher saturation ratios, digestion products were not observed. Hereafter, we reserve the term 'saturated chromatin' for those with saturation degree in the 90–128% range, 'subsaturated chromatin' for those with lower HO contents, and 'oversaturated' for higher HO loading values.

Transmission electron microscopy (TEM) and atomic force microscopy (AFM) techniques were used to confirm the formation of multiple nucleosomes on T4 DNA. Chromatin at 100% of HO loading under low salt conditions was observed as a coil-like structure (35) (Figure 3). The resolution on the TEM image (Figure 3A) allows two turns of DNA wrapped around the HO to be distinguished for the individual nucleosomes in a side view orientation. Individual nucleosomes of ca. 10 nm size (region 1) connected by a linker DNA of variable length appearing as beads-on-a-string (region 2), and as aggregated and stacked nucleosomes (region 3) were also identified on the TEM image (Figure 3A). What appears as a single chromatin molecule imaged by AFM displaying a beads-on-a-string 10 nm fiber conformation, exhibits heterogeneous distribution of nucleosomes along the DNA chain (Figure 3B). The imaged structure of recombinant T4 chromatin in this work is in agreement with the beads-on-a-string structure of 100 kb DNA reconstituted with purified HOs and imaged using AFM (17,18) and the heterogeneous structure of rat liver chromatin visualized using TEM from a recent study (36).

The T4 DNA sequence that may influence nucleosome distribution was analysed using a program optimized for *in vitro* reconstitution (31). The probability of nucleosome occupancy over the whole length of T4 DNA was observed to have a mean value of -1.8 with standard deviation ± 0.64 (Supplementary Figure S4). Occupancy values higher than 0, indicative of high affinity for nucleosome formation according to the authors' model, were not detected. The observed occupancy values in the negative range may be interpreted as sequences with nucleosome formation ability without positioning preference, which would allow random distribution of nucleosomes on the DNA for subsaturated systems. The DNA sequence should therefore not have a negative effect on nucleosome formation, because nucleosome free regions have been shown to form as a result of the action of chromatin remodelers, and not due to the DNA sequence (37). The observed nucleosome occupancy of T4 DNA, therefore leads to formation of nucleosome arrays where the degree of loading is likely to be related to the average nucleosome repeat length.

Conformational behavior of single T4 DNA molecules reconstituted with histone octamers

The long contour length of T4 DNA (ca. 60 μm) makes it possible to visualize reconstituted complexes at the level of individual molecules by fluorescence microscopy (FM) techniques. T4 DNA and chromatin complexes were labeled by the fluorescent dye YOYO and their conformational behavior was monitored in bulk solution by FM. Figure 4A shows typical snapshots of a single DNA molecule in a coil conformation exhibiting Brownian motion in a bulk solution of TE buffer with 10 mM KCl. The measured DNA long-axis length (*L*), which is defined as the longest distance in the outline of the DNA fluorescent image, is larger than the actual size by ~ 0.3 μm in each dimension (Figure 4B) due to a 'blurring effect' attributed to the resolution limit of FM (38). Upon reconstitution with HOs, the DNA coil gradually shrank (Figure 4A and C) from ca. 3.5 to 2 μm but preserved Brownian motion as well as intramolecular fluctuations.

The shrinking of DNA occurs due to the wrapping of DNA around HOs according to the well-established structure implying wrapping of ca. 50 nm of DNA length per one HO of ca. 7 nm diameter. The average values of the DNA long-axis length are plotted as a function of a loading degree in Figure 4D. As a result of nucleosome formation, the long-axis length of DNA decreased ~ 1.7-fold, which corresponds to about a 5-fold decrease of the DNA coil molecular volume. Based on FM observations, single molecules of DNA reconstituted with HOs are observed up to 128% loading. Further increase in HO loading induces intermolecular aggregation (data not shown).

Compaction of reconstituted chromatin by divalent cations

The conformation of the nucleosome arrays is strongly affected by the presence of mono- and multivalent cations (5) which have been used in studies to induce aggregation and precipitation of nucleosomes and chromatin (39–43). Therefore, the conformational behavior of chromatin reconstituted from T4 DNA in the presence of Mg^{2+} ions was studied. Figure 5 shows the dependence of the long-axis length of DNA and reconstituted chromatin on the concentration of Mg^{2+} ions in solution. According to Manning counterions condensation theory (44) that was applied to DNA in solution by Bloomfield and colleagues (45), divalent cations are unable to compact DNA because DNA anionic charges are not sufficiently neutralized by the relatively weakly bound divalent counterions. In good agreement with condensation theory and earlier experimental studies, the coil conformation of T4 DNA was preserved and the long-axis length of DNA only slightly decreased in solution with Mg^{2+} concentrations of up to 10 mM. Due to the competition of Mg^{2+} and the YOYO fluorescent dye for DNA binding, higher Mg^{2+} concentrations were not studied by FM.

The dynamic light scattering (DLS) technique was used to examine effects of higher Mg^{2+} concentrations and to gain additional information about T4 DNA phase transition at the level of the molecular ensemble. DLS results in Figure 6 indicate that no DNA phase transition occurred up to 100 mM Mg^{2+}. The conformational response of chromatin due to Mg^{2+} addition at 23% of HO loading observed by FM was similar to that of free T4 DNA (Figure 5). The DLS measurements, however, revealed an increase in scattered light intensity for chromatin at 11% and 23% of HO loading above ca. 30 mM of Mg^{2+} that may be attributed to either intermolecular aggregation or intramolecular con-
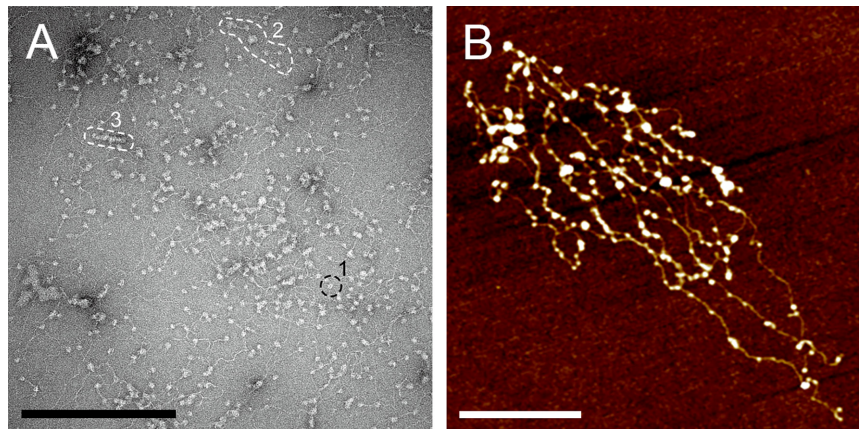
Figure 3. *In vitro* reconstituted T4 chromatin at 100% HO loading under low salt conditions were imaged as coil-like structures using TEM (**A**) and AFM (**B**). Regions 1, 2 and 3 indicate a single nucleosome, beads-on-a-string, and aggregated nucleosomes, respectively. Scale bars are 300 nm (A) and 500 nm (B).
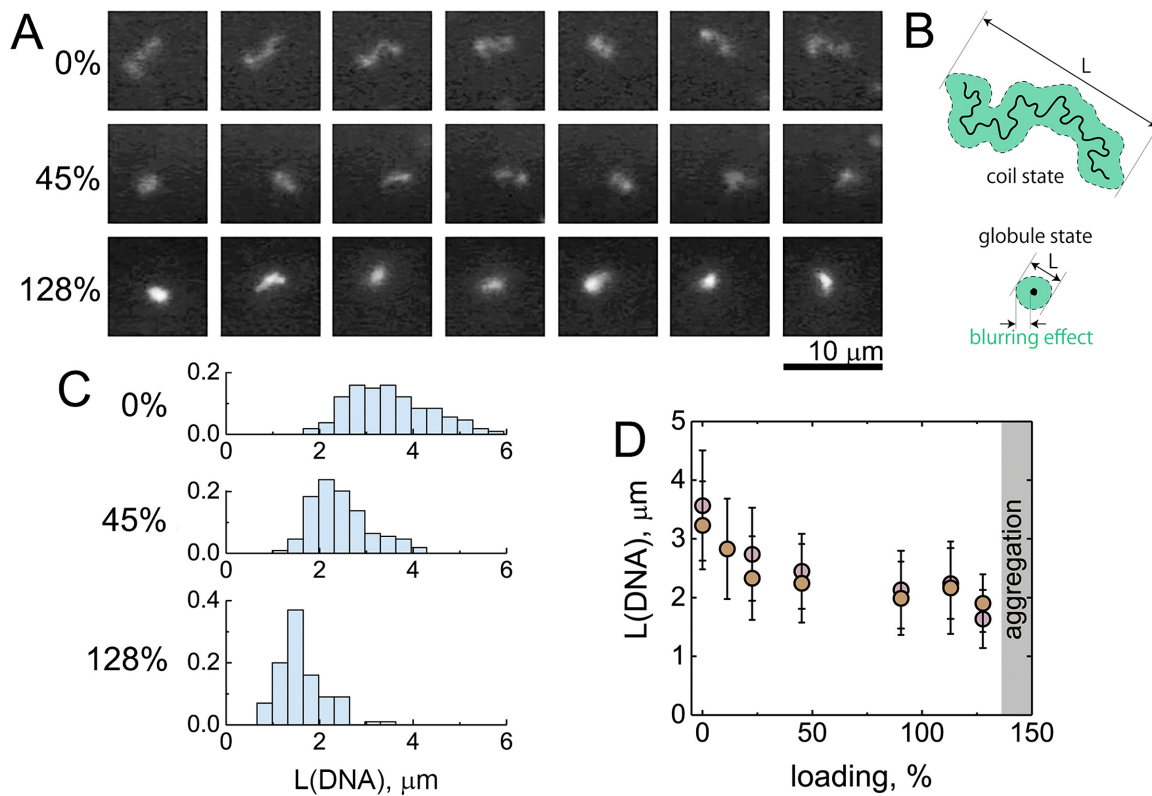

Figure 4. Single-molecule FM observations of T4 DNA conformational changes upon reconstitution with HOs. (**A**) Series of typical fluorescence micrographs of a YOYO-labeled single T4 DNA molecules and T4 DNA reconstituted with HOs at loading degrees 45% and 128% observed in a bulk solution of TE buffer with 10 mM of KCl. The time interval between snapshots is ca. 0.5 s. (**B**) Schematic representation of the relationship between actual DNA molecule in a coil or in a globule conformation and the correspondent fluorescent images, that are larger than actual DNA chain by *ca.* 0.3 μm due to blurring effect, and the definition of the characteristic parameter of long-axis length (*L*). (**C**) Long-axis length distributions of T4 DNA molecules and T4 DNA reconstituted with HOs at loading degrees 45% and 128% under conditions of A. (**D**) Changes in the average long-axis length of T4 DNA and DNA reconstituted with HOs as a function of a loading degree. Experimental points of different color correspond to two independently prepared samples. The error bars indicate the standard deviations of the average values measured over at least 100 individual DNA or chromatin molecules.
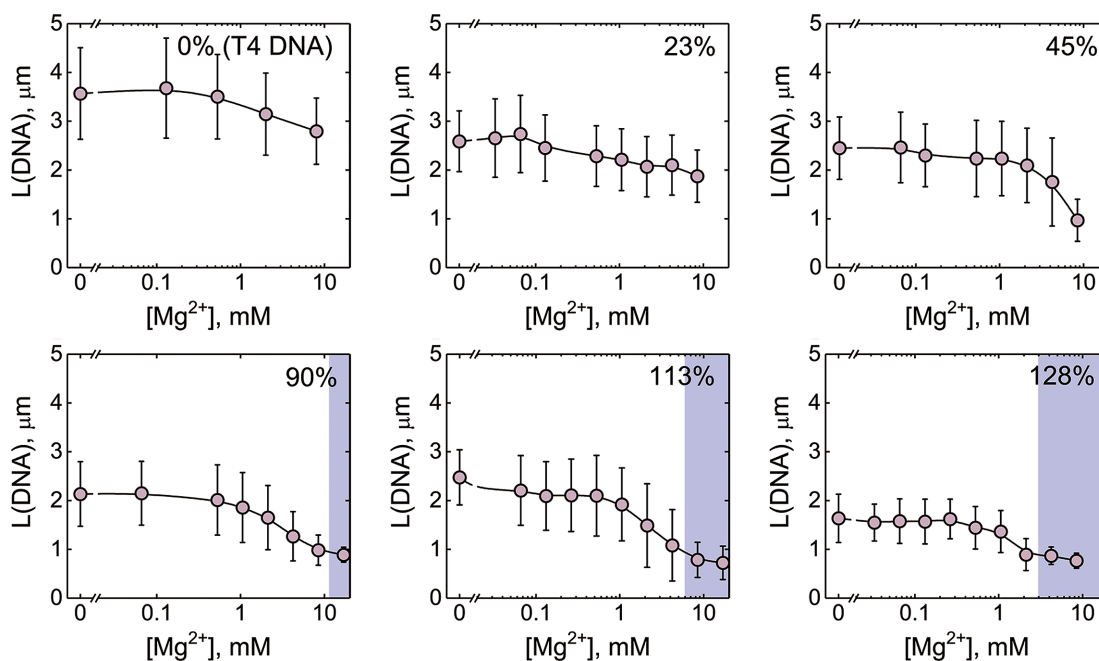
Figure 5. Compaction of T4 DNA and reconstituted chromatin by divalent cation (Mg^{2+}). Changes in the average long-axis length of YOYO-labeled T4 DNA (0.2 μM) and T4 DNA reconstituted with HOs (0.2 μM) at different loading degrees at various concentrations of magnesium chloride ($MgCl_2$) in a bulk solution of TE buffer with 10 mM of KCl. Blue areas correspond to Mg^{2+} concentrations at which DNA or chromatin molecules are completely compacted (globule state). The error bars indicate the standard deviations of the average values measured over at least 100 individual DNA or chromatin molecules.

densation. For HO loading degrees of 45% and higher, the conformational change from the unfolded coil to the compact globule and the increase in scattered light intensity were observed by FM and DLS, respectively (Figures 5 and 6). While DLS profiles for these chromatin complexes are very similar (Figure 6), single molecule FM analysis (Figure 5) shows complete compaction into globules (shaded areas) taking place at a lower concentration of Mg^{2+} ions for chromatin with higher HO loading, reaching ca. 2 mM value for the most saturated complex at 128%. The important characteristic of chromatin compaction upon addition of Mg^{2+} ion was the constant long-axis length of the chromatin coil before the onset of compaction at around 1 mM of Mg^{2+} in all samples. It should be noted, that due to a large number of HO bound to individual T4 DNA molecules, a certain heterogeneity in chromatin composition can result in a slight variation of the conformational transition point or compaction mechanism for individual chromatin molecules.

Hydrodynamic size of compacted chromatin molecules in the 90–128% HO loading range was measured by the DLS (Supplementary Figure S5A). The size of saturated chromatin remains constant, ca. 250 nm, in a rather broad concentration range of 4–60 mM Mg^{2+}, indicating the intramolecular compaction being the predominant mechanism responsible for the observed increase in scattered light intensity.

Spermine is unable to induce a first-order phase transition of chromatin

Next, we studied compaction of DNA and reconstituted chromatin by the tetravalent cation, spermine. Bearing a

charge higher than +2, spermine is able to induce compaction of free DNA by providing a sufficient charge neutralization of the DNA polyanion (45). The DLS measurements showed that T4 DNA and chromatin molecules of all studied saturation degrees underwent compaction at very similar concentrations of spermine (Supplementary Figure S6). However, the DLS method is unable to account for a far more intriguing characteristic of DNA compaction—the DNA folding scenario at the level of single DNA molecules. The striking feature of DNA compaction by tetravalent cations, the discrete conformational change at the level of single molecules, has been reported more than two decades ago (20), and in this study the mechanism of chromatin compaction was closely examined.

Figure 7 shows compaction curves for T4 DNA and chromatin of different HO loading degrees. Increase of the HO loading degree has a negligible effect on the chromatin compaction efficiency of spermine. Complete compaction of DNA and chromatin into globules of *ca.* 0.5 μm takes place at ca. 20 μM of spermine. However, the compaction mechanism for T4 DNA and chromatin at 11% HO loading was drastically different from the compaction mechanism of chromatin at loading degrees of 23% and higher. While the compaction for both T4 DNA and chromatin at 11% HO loading occurs as an all-or-none mechanism, at 23% and higher chromatin displays a continuous character of the transition.

Figures 8A and B show representative single-molecule fluorescent images of chromatin at 11% and 23% HO loading and contrast the change of DNA long-axis length distributions at different concentrations of added spermine. Compaction of chromatin at 11% takes place between 10
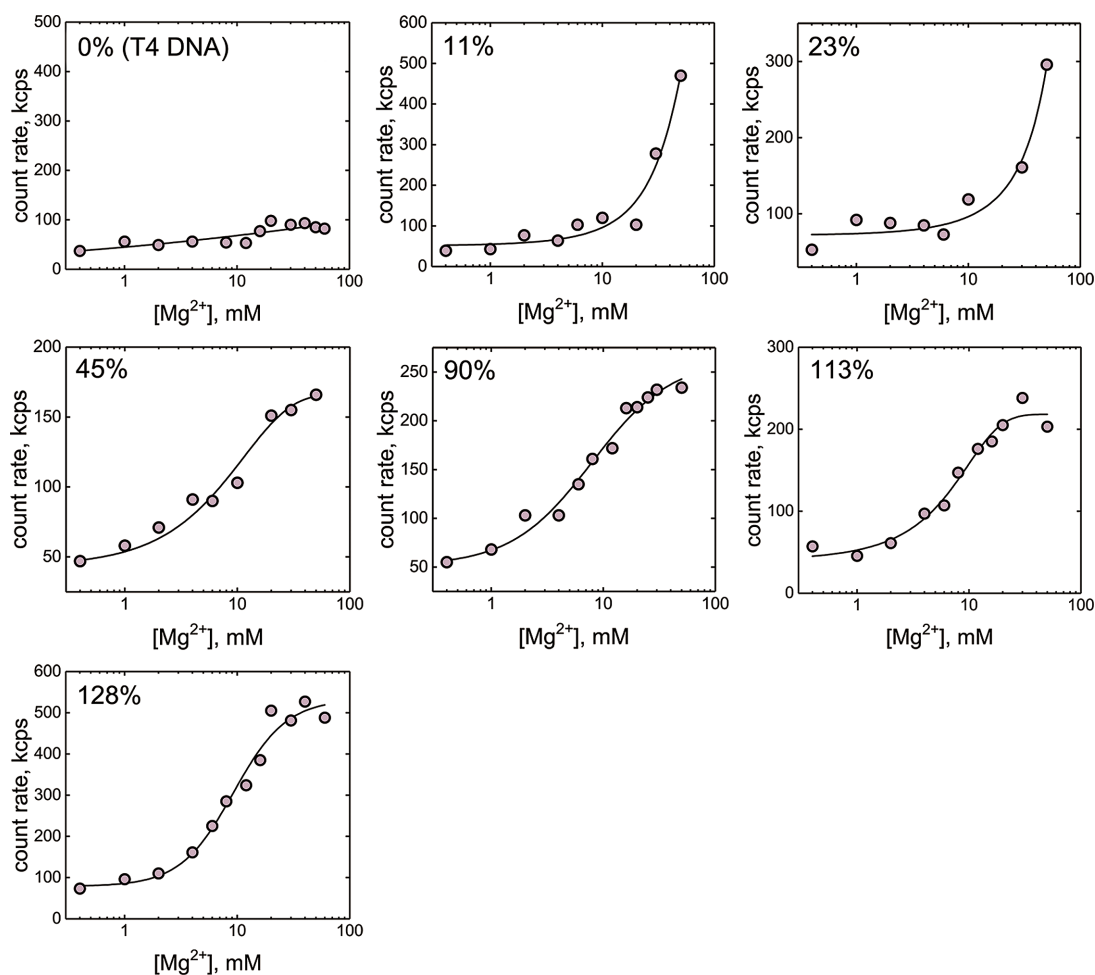
Figure 6. DLS characterization of DNA and chromatin compaction by divalent cation (Mg^{2+}). Light scattering intensity of T4 DNA molecules (2 µM) and T4 DNA reconstituted with HOs (2 µM) of different loading degrees at various concentrations of Mg^{2+} in TE buffer with 10 mM of KCl. Experimental points are measured values and curves are sigmoidal fitting of the experimental data.

and 30 µM of spermine as a first order phase transition of DNA conformation from 3.5 µm coil to 0.7 µm glob-ule through a region with a bimodal size distribution (yel-low areas on Figure 7) where coil and globule conforma-tions coexist. Coexistence of unfolded and compact forms of DNA preceding DNA collapse is a typical intermediate state in coil-globule transition of a semi-flexible long poly-electrolytes such as DNA and has been repeatedly demon-strated experimentally (46,47) and by computer simulations (48). The coexistence state appears due to double minima in the free energy profile of the DNA conformation. In contrast, the chromatin coil at 23% HO loading undergoes gradual shrinking toward compaction into a 0.7 µm glob-ular condensate (Figure 8). The increase in the HO load-ing enables chromatin to respond to the addition of small amounts of spermine by gradual compaction.

Although compaction of chromatin by spermine is de-scribed as a gradual shrinking, we noticed a large popu-lation of segregated structures in the course of the com-paction of chromatin complexes at loading degrees of 90% and higher (Figure 9). Segregated structures con-taining both coil and folded globular parts in the same DNA molecule have been reported earlier for hydrophobic

binders (49,50) and interpreted as the discrete coil-globule transition occurred within the same DNA molecule. A large fraction of molecules with intra-chain segregation observed in our system may indicate a heterogeneous HO position-ing along DNA that can cause preferential condensation of a DNA part that is more populated by HOs. Contrary to spermine, structures with intra-chain segregation were not formed during the chromatin compaction by Mg^{2+} cations, instead, the coil of DNA shrank gradually and homoge-nously to a final globular compact state.

The hydrodynamic size of the compacted chromatin com-plexes was measured by the DLS technique. Unlike chro-matin complexes compacted by Mg^{2+}, with constant hydro-dynamic size, the size of chromatin condensates compacted by spermine depends on both the degree of DNA loading with HO and the concentration of spermine (Supplemen-tary Figure S5B). Compaction of free T4 DNA yields very compact condensates of *ca.* 100 nm hydrodynamic diame-ter in good agreement with earlier studies (51). The increase of spermine concentration induced a slight increase of con-densate size to *ca.* 150 nm. It should be noted that the size of DNA condensate compacted by spermine is significantly smaller than the size of condensates compacted by Mg^{2+},
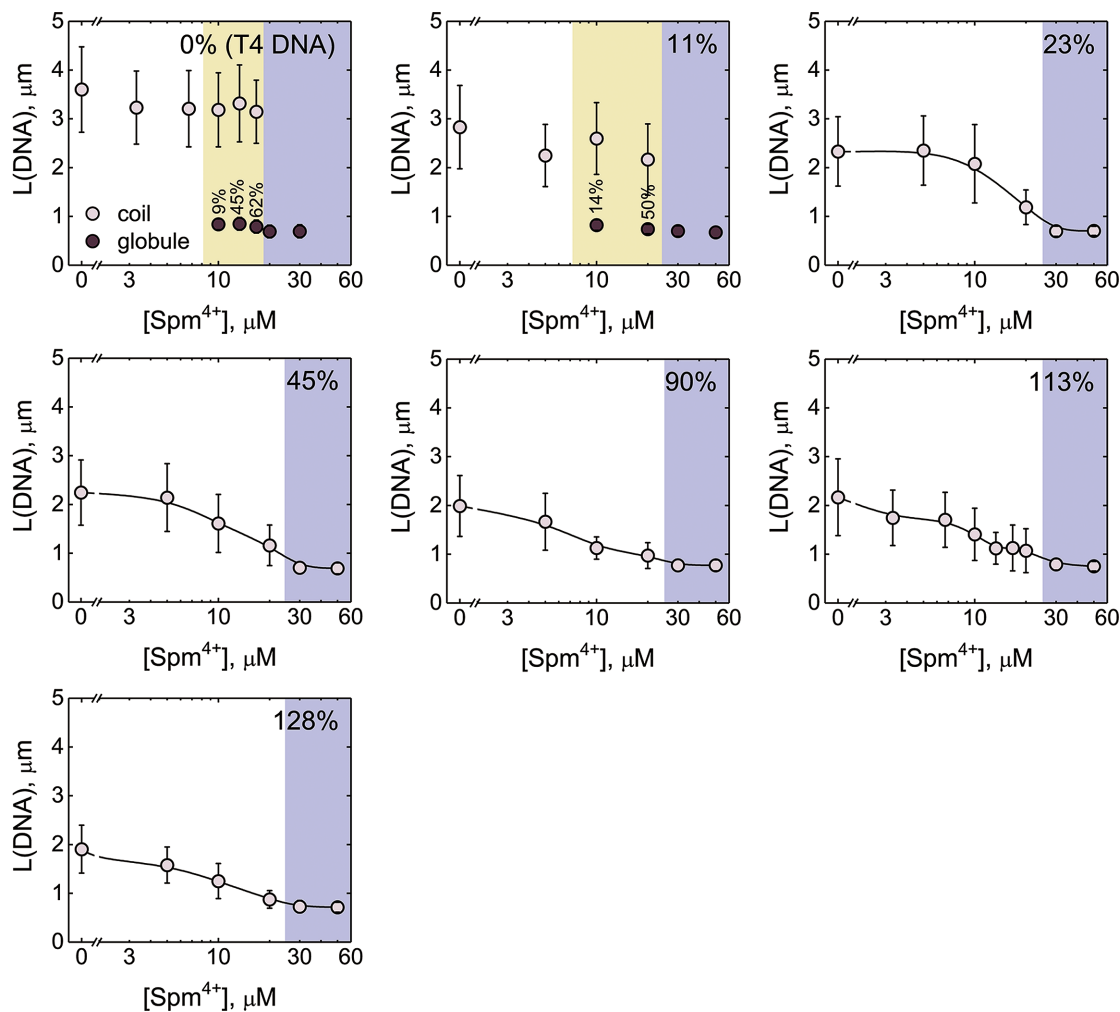
Figure 7. Compaction of T4 DNA and chromatin by tetravalent cations (spermine). Changes in the average long-axis length of YOYO-labeled T4 DNA and T4 DNA reconstituted with HOs at different loading degrees at various concentrations of tetravalent cation, spermine (Spm^{4+}), in a bulk solution of TE buffer with 10 mM KCl. Experimental points show separately the average sizes of coils and globules for T4 DNA and chromatin at 11% HO loading at intermediate spermine concentrations characterized by a bimodal distribution of DNA long-axis lengths. Yellow and blue areas are regions of coil-globule coexistence and complete DNA compaction, respectively. The error bars indicate the standard deviations of the average values measured over at least 100 individual DNA or chromatin molecules. The percentage values above experimental points in the coexistence region indicate the percentage of T4 DNA or reconstituted chromatin in the compact state.

i.e. 250 nm. Because the compaction of DNA and chromatin by spermine takes place in the same concentration range of spermine between 10 and 100 μM (Supplementary Figure S6) one can compare the hydrodynamic sizes of chromatin of different HO loading degree at a certain concentration of spermine. From Supplementary Figure S5B it is clear that the average size of the DNA condensate grows with an increase of the loading degree. On the other hand, all the complexes have the same trend to increase condensate size with the increase of spermine concentration. This increase is more notable for complexes at higher loading degrees and reaches 300–400 nm size. The increase of DNA condensate size may be ascribed to the overcharging of nucleosomes by spermine (40) resulting in strong intramolecular repulsion and swelling of compact condensates. A contribution of intermolecular aggregation to the increase in size cannot be ruled out.

DISCUSSION

The higher-order structure of chromatin and its manner of compaction are closely associated with its genetic activity in cells (52–54). However, while our present understanding of chromatin condensation/compaction mainly comes from *in vitro* studies on well-defined systems based on short nucleosomal arrays with nucleosome positioning sequences (55), the chromatin *in vivo* contains significantly longer DNA chains (up to hundreds of thousands bp in a single chromosome loop) (56) folded hierarchically into heteromorphic structures (57), with the majority of nucleosomes positioned irregularly (26,36,58,59). Therefore, studies of chromatin reconstituted on large DNA molecules without nucleosome positioning will improve our understanding of chromatin properties *in vivo*.

FM observations show that 165.6 kb giant DNA folding into chromatin is accompanied by a gradual shrink-
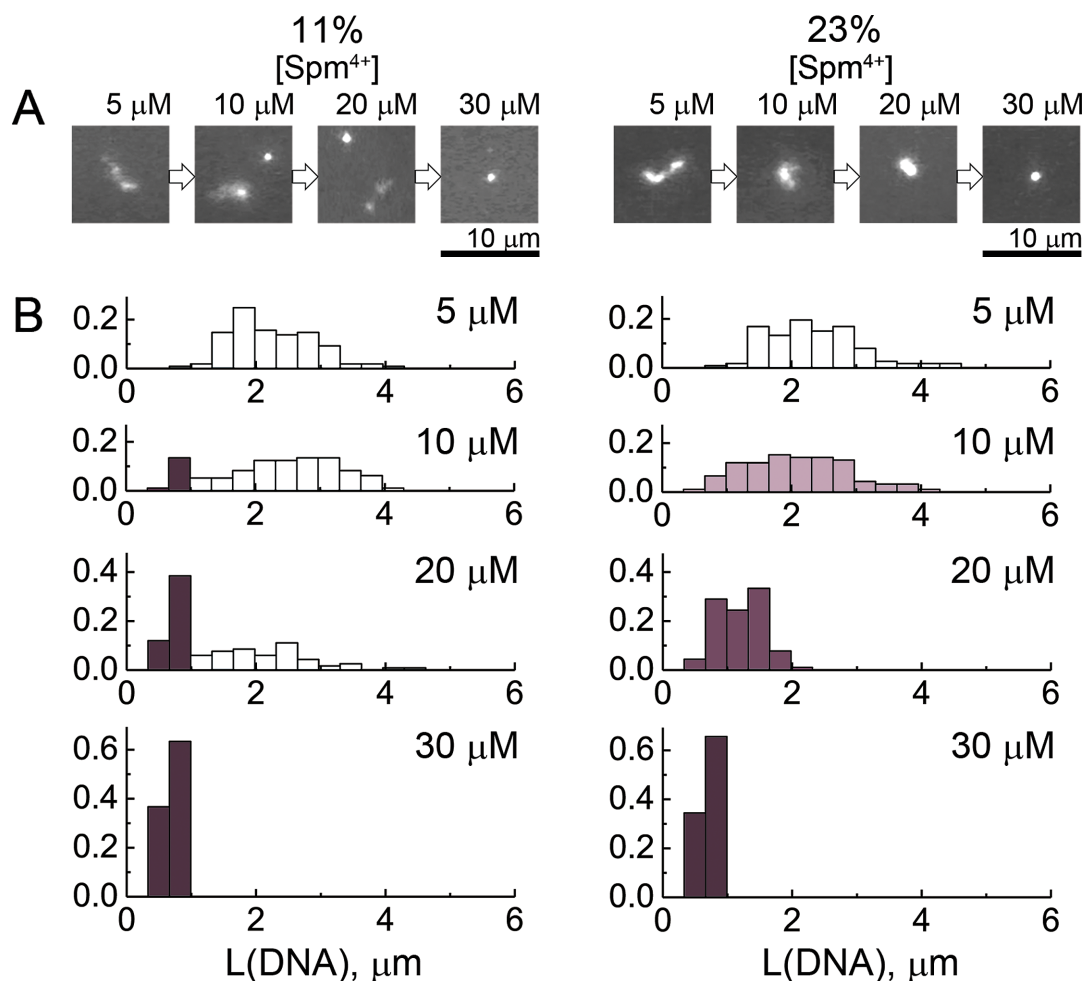
Figure 8. Two compaction scenarios of T4 chromatin by a tetracation. (**A**) Typical fluorescence micrographs of a YOYO-labelled T4 DNA reconstituted with HOs at 11% (left) and 23% (right) loading degrees, observed at different concentrations of spermine in a bulk solution of TE buffer with 10 mM of KCl. The concentrations of spermine are indicated above corresponding images. (**B**) Long-axis length distributions of chromatin at 11% (left) and 23% (right) loading degrees under conditions of A.
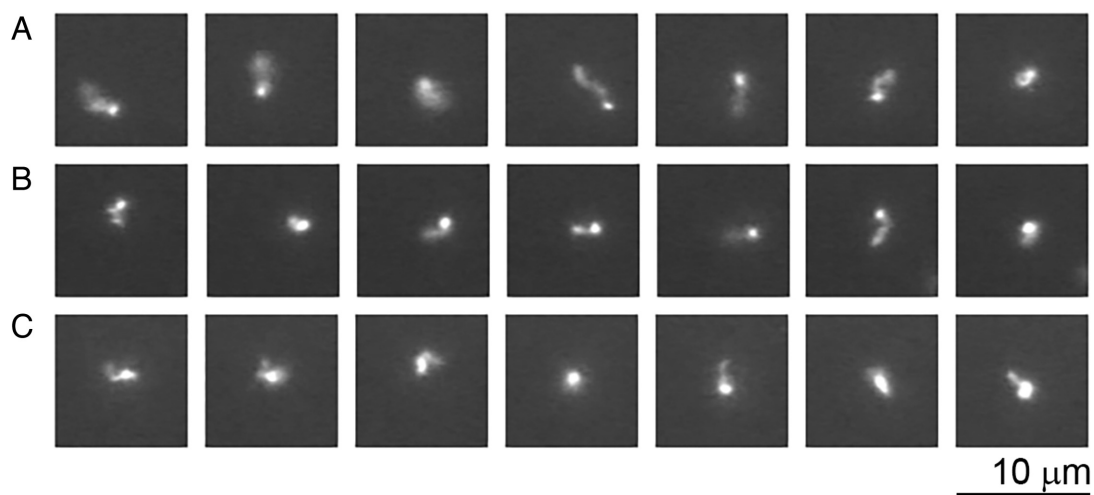

Figure 9. Formation of intrachain segregation structures during compaction of reconstituted chromatin. Series of typical fluorescence micrographs of a YOYO-labelled chromatin at 113% loading degree in the presence of 6.7 μM spermine in a bulk solution of TE buffer with 10 mM of KCl. The time interval between snapshots is *ca.* 0.5 sec.

ing of the DNA coil dependent on the HO loading (Figure 4). At the level of the resolution of the FM experiment, the fluorescence intensity was homogeneously distributed along individual coils of both subsaturated and saturated chromatin molecules, indicating no strong heterogeneity of nucleosome density along DNA chains and the sequence-based probability of nucleosome occupancy (Supplementary Figure S4). However, the HO positioning on the DNA chain was characterized by a certain heterogeneity manifested in a difference in linker DNA length (Figure 3). Oversaturation of DNA with HOs induces intermolecular aggregation, likely involving nonspecific binding of HOs to DNA and nucleosomes.

The bioavailable polycations Mg^{2+} and spermine exist at millimolar concentrations in the living cell (60,61), thus they can be directly involved in regulation of chromatin higher-order structure *in vivo*. Although one may expect similar trends in compaction of negatively charged chromatin by di- and tetravalent cations as a result of neutralization of negatively charged DNA phosphates, our results reveal a considerable difference between the effects of divalent magnesium cations and tetravalent spermine cations on the higher-order structure of subsaturated and saturated nucleosomal arrays, in agreement with cation-dependent effects reported earlier (43).

The protection from MNase digestion indicates the compacted state of chromatin. The observed protection of chromatin may result from the close positioning of nucleosomes on DNA, and nonspecific binding of histones. Furthermore, the presence of 5 mM Ca^{2+} cations in the MNase reaction buffer augments compaction and aggregation. Compacted chromatin globules were observed in the millimolar range of Mg^{2+} concentrations by FM in this work (Figure 5). For oversaturated chromatin, at ratios higher than 131% the excess cationic HOs may bind non-specifically to the negatively charged chromatin fibers, leading to chromatin neutralization and aggregation. At degrees of HO loading above 128%, the chromatin may represent a beads-on-a-string structure with very close-packed nucleosomes, which may not be the most physiologically relevant complex. Although telomeric chromatin has been shown to have 157 nucleosome repeat length (62), the majority of eukaryotic chromatin has a nucleosome every 200 ± 40 bp (63).

Chromatin compaction by magnesium ions

Mg^{2+} ions do not induce condensation of double-stranded DNA because its electrostatic interaction with DNA does not provide sufficient DNA charge neutralization (64). On the other hand, Mg^{2+} is known to effectively promote condensation/aggregation of nucleosomes and nucleosome arrays (42,65). Thus, Mg^{2+}-induced aggregation of nucleosomes, in which the DNA's charge is partly neutralized by cationic histone octamers (40), is due to attractive interactions. Attractive interactions between nucleosomes in chromatin originate from the ion-ion correlation effects (66) due to a positional correlation of Mg^{2+} ions condensed on different adjacent negatively charged segments of DNA (67) in nucleosomes, coupled with histone tail bridging (5). A certain contribution to minimize the free energy in the chromatin compaction process originates from an increase of

translational entropy of counterions (68) released during chromatin compaction and effects associated with cationic tails (69).

Because the saturated chromatin can be compacted by Mg^{2+} in contrast to 'naked' DNA (Figure 5), the degree of chromatin saturation by histones is clearly the factor that determines the ability of a divalent cation to compact chromatin. Indeed, in earlier systematic studies on subsaturated nucleosome arrays, the degree of saturation was shown to play a crucial role in the chromatin condensation (70). The condensation of subsaturated chromatin by Mg^{2+} was significant only if saturation degrees were higher than ca. 70% (70,71). This saturation degree threshold was explained based on pairwise preference in nucleosome occupation (72). These studies emphasized the importance of adjacent nucleosomes interaction for chromatin condensation. The saturation degrees above ca. 70% imply the absence of large gaps between adjacent nucleosomes providing effective inter-nucleosomal interactions through histone cationic tails leading to the efficient chromatin condensation.

The long chromatin compaction in our study has many similarities with earlier results on well-defined short nucleosome arrays. Free DNA is not compacted by divalent cations (Figures 5 and 6). Due to the relatively weak interaction of Mg^{2+} ions with both DNA and nucleosomes, the conformation of chromatin remains virtually unchanged until millimolar amounts of Mg^{2+} are added to induce association of the nucleosomes. In contrast to short fragments of subsaturated chromatin (70,71), Mg^{2+} induced condensation of highly unsaturated chromatin at 11% of HO loading was detected by DLS technique (Figure 6), but at Mg^{2+} concentrations 10 times higher than sufficient to induce the compaction of the saturated chromatin at 113% and 128%. The concentration of Mg^{2+} needed to induce single-molecule compaction of chromatin with loading higher than 40% decreased moderately and approached concentration of several mM – typical Mg^{2+} concentration to induce association of saturated nucleosome arrays (73,74) or aggregation of nucleosomes in solution (65). Despite the very low concentrations used here for megabase-long chromatin in the FM observations, the compaction behavior is similar to the intermolecular self-association (aggregation) observed for reconstituted 12-mer arrays using the '601' positioning sequence (67). The onset and the cooperativity of nucleosome array aggregation and the compaction of single chromatin molecules of high saturation degree occur at comparable Mg^{2+} concentrations. Condensation of chromatin begins in both cases at *ca.* 1 mM of Mg^{2+} added to the solution and ended at 4 mM Mg^{2+} for 12-mer nucleosomal array (74) and at 4–7 mM for saturated T4 chromatin (Figures 5 and 6).

The results above clearly show that the high degree of chromatin saturation is the essential condition for efficient chromatin compaction by Mg^{2+} regardless of chromatin length. Nevertheless, compaction of long chromatin by Mg^{2+} can be achieved even at low degrees of saturation, at which short nucleosome arrays associate poorly (75). This observation may be relevant for chromatin in the cell, where chromatin containing several hundreds of nucleosomes may have the histone-depleted DNAs regions

in a compacted state because of a sufficient number of nucleosome-nucleosome attractive interactions.

In a recent paper, Maeshima et al. investigated condensation of short nucleosomal arrays by Mg^{2+} cations and found that a great number of molecules cooperatively assemble into globular condensates with sizes between 50 and 1000 nm [76]. In contrast, under the present conditions, compaction of megabase-long chromatin, induced by Mg^{2+} occurs as a single molecule event resulting in formation of globules of ca. 250 nm with no detectable aggregation tendency into larger condensates. The main reason is that under the present conditions of very low DNA concentration, monomolecular collapse of chromatin is thermodynamically preferred to intermolecular aggregation [77–79]. Despite the general agreement in concentration ranges of Mg^{2+} and sizes of aggregates observed in both studies, the long DNA used in our work may be more biologically relevant, thus being a suitable *in vitro* model system to study chromosome structure and functions.

Previous studies of native chromatin containing ∼40 nucleosomes per DNA chain also acknowledged the formation of 30 nm chromatin fibers [80] preceding compaction of chromatin into globules, yet the relevance of 30 nm fiber to chromosome assembly *in vivo* is recently under debate in the field [81]. Chromatin compaction profiles (Figure 5) and DLS data (Figure 6) show the saturated chromatin coil undergoing a gradual decrease in size while it turns into a globule. DLS measurements of the hydrodynamic radii (Supplementary Figure S5A) revealed only one type of compact condensate of several hundred nanometers in size, which corresponds to a globular form of condensed chromatin. All these observations support a model of direct folding of dynamic 10-nm chromatin fiber into a globular condensate although the formation of regions of 30 nm fiber may not be ruled out.

Chromatin compaction by spermine

Compaction of chromatin by tetravalent cations is drastically different from Mg^{2+}-induced compaction. Considering the purely electrostatic effect of spermine on nucleosome aggregation, it is clear that spermine induces nucleosome aggregations at lower concentrations than Mg^{2+}. According to Manning's theory [44], the fraction of neutralized charges on free DNA is equal to 94% in the presence of tetravalent cations, which is sufficient to induce DNA compaction that requires *ca.* 91% charge neutralization [64]. The same theory gives 96% of phosphates neutralized by spermine for DNA in nucleosomes [40]. Consequently, not only spermine can induce aggregation of nucleosomes as we discussed for Mg^{2+}-induced chromatin compaction, but its interaction with DNA can also largely promote attractive interactions between segments of free DNA. Because the neutralization of free DNA charges and DNA in nucleosomes by spermine is of the same degree, free DNA and chromatin of different saturation degree should fold at approximately the same amount of added spermine to solution. Both DLS and FM studies show constant spermine concentration (*ca.* 20 µM) at which DNA and chromatin are folded into compact globules (Figure 7 and Supplementary Figure S6).

There is, however, a fundamental difference between the compaction mechanisms at the level of single molecules. The free DNA undergoes a discrete coil-globule transition [20], whereas the saturated chromatin is observed to shrink gradually (Figures 8 and 9). For subsaturated chromatin samples, the change of compaction mechanism from discrete to continuous occurs between 11% and 23% of HO loading (Figure 7).

Earlier studies have shown that when a polymer chain is rigid enough, its folding transition occurs in a discrete manner [82], whereas the transition is continuous for flexible polymeric chain. Free DNA with a persistence length of 50 nm [83] is classified as a relatively rigid (or semi-flexible) polymer chain, while the nucleosomal arrays and chromatin are more flexible with a persistence length <30 nm according to single-molecule experiments [84,85]. Therefore, the alteration of the effective persistence length of DNA by the degree of histone saturation is expected to affect the manner of chromatin folding by multivalent cations. On the other hand, the difference between the average length of nucleosome-free DNA fragments in subsaturated chromatin may also be a factor to switch the DNA compaction mechanism in the following way. The all-or-none DNA compaction may be preceded by the formation of a nucleation loop of DNA around which the remaining chain of DNA is wound up forming highly ordered, crystal-like toroidal condensate [51,86,87]. The size of the DNA toroidal condensate is determined by the DNA mechanical and electrostatic rigidity and it is usually in a range of 50–70 nm in diameter [88]. One loop of the toroidal DNA condensate corresponds to ∼150–200 nm of DNA length. Consequently, histone-free DNA fragments in chromatin at 11% loading can form a nucleation center containing 3 loops of wound DNA to induce compaction of the remained chain. In contrast, the subsaturated chromatin at 23% contains twice shorter fragments of free DNA (250 nm in average) that can form only one full loop, which is unstable to serve as a nucleation center and initiate all-or-none type of DNA folding [89].

The discrete transition of the DNA coil to a globule results in a very tight packaging of DNA similar to the DNA packaging in bacteriophage heads [90] and causes a complete inhibition of DNA transcriptional activity [91]. In this regard, DNA binding with only 20% of HO compared to the saturation amount leads to a change in DNA compaction scenario that may allow for a more flexible regulation of DNA genetic activity in eukaryotic cells.

Another important feature of chromatin compaction by spermine revealed in our FM study is a strong intra-chain segregation along individual chromatin molecules with a high degree of nucleosome saturation (Figure 9). In aggregation studies of short chromatin fragments, it was demonstrated that DNA saturation by HO is a stochastic process at low and medium saturation degrees, while a certain weak cooperativity is manifested at high saturation degrees due to pairwise preference in nucleosome occupation [72] caused by histone tail interactions [92]. Atomic force microscopy studies by Yoshikawa et al. also revealed a bimodal profile of nucleosome densities along reconstituted chromatin of high saturation degrees [52], that supports the mechanism of a cooperative HO binding when the density of HO is

high. Therefore, one may expect that chromatin at HO loading 90% and higher possesses a certain degree of heterogeneity in terms of nucleosome density. This heterogeneity leads to a fluctuation in a charge density and, probably, structure of chromatin along the same DNA that causes a difference in chromatin compaction states at the same concentration of multivalent cation. In good agreement with this model, strong intra-chain segregation was observed only for chromatin with high degree of saturation (90% and higher) while no intra-chain segregation was observed for subsaturated chromatin. This phenomenon might have an important implication to gene regulation: cooperative nucleosome positioning may result in more efficient compaction of such chromosomal regions resulting in suppression of genes over a significant DNA length. The observation of intrachain segregation or nucleosome clustering observed in our recombinant system by FM and AFM, may mimic the organization of chromatin *in situ* (59) and 'nucleosome clutching' (58) reported recently. A thorough characterization of our model system is needed before a mechanism responsible for nucleosome segregation and its relevance to the *in vivo* chromatin structure and function can be established.

We noted that intra-chain segregation was observed only in chromatin compaction by spermine, but not by Mg^{2+}. This difference can be explained by insufficient stabilization of a compact chromatin phase due to weak condensation potency of Mg^{2+} in comparison with spermine. Sperminemediated compaction, in turn, better mimics chromatin compaction in nuclei by polycations, like histone tails, and linker histones.

CONCLUSIONS

By single-molecule observations of DNA and chromatin interacting with multivalent cations, we uncovered hitherto unknown features of unimolecular DNA compaction. The most important findings are the following: (i) Complexation of DNA with a small fraction (10–20%) of histones is sufficient to induce DNA compaction by adding divalent cations such as Mg^{2+}. (ii) Complexation of DNA with a small fraction (*ca.* 20%) of histones is sufficient to change the first-order DNA compaction transition into a gradual shrinking to a compact globule. (iii) Compaction of saturated chromatin by spermine proceeds through intrachain segregation in single DNA molecules containing unfolded and compact parts in the same chain. This first study of reconstituted chromatin of size similar to TADs, i.e. nearly megabase length of DNA and *ca.* 300 nm size of chromatin condensate, is a step forward to reproducing the state of chromatin in the nucleus and hence of great biological relevance as a model for chromatin condensation *in vivo*. Studies on genome-wide nucleosome positioning revealed that most of eukaryotic chromatin is heterogeneous and does not show regular nucleosome positioning on the same DNA sequences in different cell types or during cell development stages or on functionally similar DNA sequences (26). Therefore, the somewhat heterogeneous chromatin reconstituted on a long nonspecific DNA template like T4 DNA in the present study, should be a more relevant *in vivo* model for chromatin formed on large megabase size DNA, compared to saturated nucleosomal arrays with regular NRL, constructed using DNA template based on high affinity nucleosome positioning sequences, which are limited in size.

SUPPLEMENTARY DATA

Supplementary Data are available at NAR Online.

REFERENCES

1. Luger,K., Mader,A.W., Richmond,R.K., Sargent,D.F. and Richmond,T.J. (1997) Crystal structure of the nucleosome core particle at 2.8 angstrom resolution. *Nature*, **389**, 251–260.
2. Davey,C.A., Sargent,D.F., Luger,K., Maeder,A.W. and Richmond,T.J. (2002) Solvent mediated interactions in the structure of the nucleosome core particle at 1.9 angstrom resolution. *J. Mol. Biol.*, **319**, 1097–1113.
3. Bannister,A.J. and Kouzarides,T. (2011) Regulation of chromatin by histone modifications. *Cell Res.*, **21**, 381–395.
4. Talbert,P.B. and Henikoff,S. (2017) Histone variants on the move: substrates for chromatin dynamics. *Nat. Rev. Mol. Cell. Biol.*, **18**, 115–126.
5. Korolev,N., Allahverdi,A., Lyubartsev,A.P. and Nordenskiold,L. (2012) The polyelectrolyte properties of chromatin. *Soft Matter*, **8**, 9322–9333.
6. Schiessel,H. (2003) The physics of chromatin. *J. Phys. Condens. Mat.*, **15**, R699–R774.
7. Schalch,T., Duda,S., Sargent,D.F. and Richmond,T.J. (2005) X-ray structure of a tetranucleosome and its implications for the chromatin fibre. *Nature*, **436**, 138–141.
8. Robinson,P.J., Fairall,L., Huynh,V.A. and Rhodes,D. (2006) EM measurements define the dimensions of the "30-nm" chromatin fiber: evidence for a compact, interdigitated structure. *PNAS*, **103**, 6506–6511.
9. Routh,A., Sandin,S. and Rhodes,D. (2008) Nucleosome repeat length and linker histone stoichiometry determine chromatin fiber structure. *PNAS*, **105**, 8872–8877.
10. Jiang,C.Z. and Pugh,B.F. (2009) Nucleosome positioning and gene regulation: advances through genomics. *Nat. Rev. Genet.*, **10**, 161–172.
11. Dekker,J. (2014) Two ways to fold the genome during the cell cycle: insights obtained with chromosome conformation capture. *Epigenet. Chromatin*, **7**, 25.
12. Fraser,J., Williamson,I., Bickmore,W.A. and Dostie,J. (2015) An overview of genome organization and how we got there: from FISH to Hi-C. *Microbiol. Mol. Biol. Rev.*, **79**, 347–372.

13. Cremer,T. and Cremer,M. (2010) Chromosome territories. *Cold. Spring Harb. Perspect. Biol.*, **2**, a003889.
14. Dixon,J.R., Selvaraj,S., Yue,F., Kim,A., Li,Y., Shen,Y., Hu,M., Liu,J.S. and Ren,B. (2012) Topological domains in mammalian genomes identified by analysis of chromatin interactions. *Nature*, **485**, 376–380.
15. Nora,E.P., Lajoie,B.R., Schulz,E.G., Giorgetti,L., Okamoto,I., Servant,N., Piolot,T., Berkum,N.L., Meisig,J. and Sedat,J. (2012) Spatial partitioning of the regulatory landscape of the X-inactivation centre. *Nature*, **485**, 381–385.
16. Wachsmuth,M., Knoch,T.A. and Rippe,K. (2016) Dynamic properties of independent chromatin domains measured by correlation spectroscopy in living cells. *Epigenet. Chromatin*, **9**, 57.
17. Hizume,K., Yoshimura,S.H. and Takeyasu,K. (2004) Atomic force microscopy demonstrates a critical role of DNA superhelicity in nucleosome dynamics. *Cell Biochem. Biophys.*, **40**, 249–261.
18. Hizume,K., Yoshimura,S.H. and Takeyasu,K. (2005) Linker histone H1 per se can induce three-dimensional folding of chromatin fiber. *Biochemistry*, **44**, 12978–12989.
19. Yoshikawa,K. (2001) Controlling the higher-order structure of giant DNA molecules. *Adv. Drug. Deliver. Rev.*, **52**, 235–244.
20. Yoshikawa,K., Takahashi,M., Vasilevskaya,V.V. and Khokhlov,A.R. (1996) Large discrete transition in a single DNA molecule appears continuous in the ensemble. *Phys. Rev. Lett.*, **76**, 3029–3031.
21. Tsumoto,K., Luckel,F. and Yoshikawa,K. (2003) Giant DNA molecules exhibit on/off switching of transcriptional activity through conformational transition. *Biophys. Chem.*, **106**, 23–29.
22. Huang,Y.C., Su,C.J., Chen,C.Y., Chen,H.L., Jeng,U.S., Berezhnoy,N.V., Nordenskiold,L. and Ivanov,V.A. (2016) Elucidating the DNA-histone interaction in nucleosome from the DNA-dendrimer complex. *Macromolecules*, **49**, 4277–4285.
23. Zinchenko,A.A., Sakaue,T., Araki,S., Yoshikawa,K. and Baigl,D. (2007) Single-chain compaction of long duplex DNA by cationic nanoparticles: Modes of interaction and comparison with chromatin. *J. Phys. Chem. B*, **111**, 3019–3031.
24. Zinchenko,A.A., Yoshikawa,K. and Baigl,D. (2005) Compaction of single-chain DNA by histone-inspired nanoparticles. *Phys. Rev. Lett.*, **95**, 228101.
25. Takenaka,Y., Nagahara,H., Kitahata,H. and Yoshikawa,K. (2008) Large-scale on-off switching of genetic activity mediated by the folding-unfolding transition in a giant DNA molecule: An hypothesis. *Phys. Rev. E*, **77**, 031905.
26. Valouev,A., Johnson,S.M., Boyd,S.D., Smith,C.L., Fire,A.Z. and Sidow,A. (2011) Determinants of nucleosome organization in primary human cells. *Nature*, **474**, 516–520.
27. Berezhnoy,N.V., Lundberg,D., Korolev,N., Lu,C., Yan,J., Miguel,M., Lindman,B. and Nordenskiöld,L. (2012) Supramolecular organization in self-assembly of chromatin and cationic lipid bilayers is controlled by membrane charge density. *Biomacromolecules*, **13**, 4146–4157.
28. Dorigo,B., Schalch,T., Bystricky,K. and Richmond,T.J. (2003) Chromatin fiber folding: requirement for the histone H4N-terminal tail. *J. Mol. Biol.*, **327**, 85–96.
29. Huynh,V.A., Robinson,P.J. and Rhodes,D. (2005) A method for the in vitro reconstitution of a defined "30 nm" chromatin fibre containing stoichiometric amounts of the linker histone. *J. Mol. Biol.*, **345**, 957–968.
30. Muthurajan,U., Mattiroli,F., Bergeron,S., Zhou,K., Gu,Y., Chakravarthy,S., Dyer,P., Irving,T. and Luger,K. (2016) In: Ronen,M (ed). *Methods Enzymol*. Academic Press, Vol. **573**, pp. 3–41.
31. van der Heijden,T., van Vugt,J.J.F.A., Logie,C. and van Noort,J. (2012) Sequence-based prediction of single nucleosome positioning and genome-wide nucleosome occupancy. *PNAS*, **109**, 2514–2522.
32. Meng,H., Andresen,K. and van Noort,J. (2015) Quantitative analysis of single-molecule force spectroscopy on folded chromatin fibers. *Nucleic Acids Res.*, **43**, 3578–3590.
33. Cuatrecasas,P., Fuchs,S. and Anfinsen,C.B. (1967) Catalytic properties and specificity of the extracellular nuclease of Staphylococcus aureus. *J. Biol. Chem.*, **242**, 1541–1547.
34. Galati,A., Micheli,E., Alicata,C., Ingegnere,T., Cicconi,A., Pusch,M.C., Giraud-Panis,M.J., Gilson,E. and Cacchione,S. (2015) TRF1 and TRF2 binding to telomeres is modulated by nucleosomal organization. *Nucleic Acids Res.*, **43**, 5824–5837.
35. Thoma,F., Koller,T. and Klug,A. (1979) Involvement of histone-H1 in the organization of the nucleosome and of the salt-dependent superstructures of chromatin. *J. Cell Biol.*, **83**, 403–427.
36. Ehrensberger,A.H., Franchini,D.M., East,P., George,R., Matthews,N., Maslen,S.L. and Svejstrup,J.Q. (2015) Retention of the native epigenome in purified mammalian chromatin. *PLoS One*, **10**, e0133246.
37. Lorch,Y., Maier-Davis,B. and Kornberg,R.D. (2014) Role of DNA sequence in chromatin remodeling and the formation of nucleosome-free regions. *Genes Dev.*, **28**, 2492–2497.
38. Yoshikawa,K. and Matsuzawa,Y. (1995) Discrete phase transition of giant DNA dynamics of globule formation from a single molecular chain. *Physica D*, **84**, 220–227.
39. Fredericq,E., Hacha,R., Colson,P. and Houssier,C. (1991) Condensation and precipitation of chromatin by multivalent cations. *J. Biomol. Struct. Dyn.*, **8**, 847–865.
40. Raspaud,E., Chaperon,I., Leforestier,A. and Livolant,F. (1999) Spermine-induced aggregation of DNA, nucleosome, and chromatin. *Biophys. J.*, **77**, 1547–1555.
41. Korolev,N., Allahverdi,A., Yang,Y., Fan,Y.P., Lyubartsev,A.P. and Nordenskiold,L. (2010) Electrostatic origin of salt-induced nucleosome array compaction. *Biophys. J.*, **99**, 1896–1905.
42. Hansen,J.C. (2002) Conformational dynamics of the chromatin fiber in solution: determinants, mechanisms, and functions. *Annu. Rev. Bioph. Biom.*, **31**, 361–392.
43. Berezhnoy,N.V., Liu,Y., Allahverdi,A., Yang,R., Su,C.-J., Liu,C.-F., Korolev,N. and Nordenskiöld,L. (2016) The influence of ionic environment and histone tails on columnar order of nucleosome core particles. *Biophys. J.*, **110**, 1720–1731.
44. Manning,G.S. (1978) Molecular theory of polyelectrolyte solutions with applications to electrostatic properties of polynucleotides. *Q. Rev. Biophys.*, **11**, 179–246.
45. Wilson,R.W. and Bloomfield,V.A. (1979) Counter-ion-induced condensation of deoxyribonucleic-acid - light-scattering study. *Biochemistry*, **18**, 2192–2196.
46. Melnikov,S.M., Sergeyev,V.G. and Yoshikawa,K. (1995) Discrete coil-globule transition of large DNA induced by cationic surfactant. *J. Am. Chem. Soc.*, **117**, 2401–2408.
47. Takahashi,M., Yoshikawa,K., Vasilevskaya,V.V. and Khokhlov,A.R. (1997) Discrete coil-globule transition of single duplex DNAs induced by polyamines. *J. Phys. Chem. B*, **101**, 9396–9401.
48. Sarraguca,J.M., Dias,R.S. and Pais,A.A. (2006) Coil-globule coexistence and compaction of DNA chains. *J. Biol. Phys.*, **32**, 421–434.
49. Zinchenko,A.A., Sergeyev,V.G., Murata,S. and Yoshikawa,K. (2003) Controlling the intrachain segregation on a single DNA molecule. *J. Am. Chem. Soc.*, **125**, 4414–4415.
50. Chen,N., Zinchenko,A.A., Murata,S. and Yoshikawa,K. (2005) Specific formation of beads-on-a-chain structures on giant DNA using a designed polyamine derivative. *J. Am. Chem. Soc.*, **127**, 10910–10916.
51. Hud,N.V. and Vilfan,I.D. (2005) Toroidal DNA condensates: Unraveling the fine structure and the role of nucleation in determining size. *Annu. Rev. Bioph. Biom.*, **34**, 295–318.
52. Nakai,T., Hizume,K., Yoshimura,S.H., Takeyasu,K. and Yoshikawa,K. (2005) Phase transition in reconstituted chromatin. *Europhys. Lett.*, **69**, 1024–1030.
53. Li,G.H. and Reinberg,D. (2011) Chromatin higher-order structures and gene regulation. *Curr. Opin. Genet. Dev.*, **21**, 175–186.
54. Horn,P.J. and Peterson,C.L. (2002) Molecular biology: Chromatin higher order folding: wrapping up transcription. *Science*, **297**, 1824–1827.
55. Robinson,P.J.J. and Rhodes,D. (2006) Structure of the '30 nm' chromatin fibre: a key role for the linker histone. *Curr. Opin. Struc. Biol.*, **16**, 336–343.
56. Jackson,D.A., Dickinson,P. and Cook,P.R. (1990) The size of chromatin loops in HeLa-cells. *EMBO J.*, **9**, 567–571.
57. Grigoryev,S.A., Arya,G., Correll,S., Woodcock,C.L. and Schlick,T. (2009) Evidence for heteromorphic chromatin fibers from analysis of nucleosome interactions. *PNAS*, **106**, 13317–13322.
58. Ricci,M.A., Manzo,C., Garcia-Parajo,M.F., Lakadamyali,M. and Cosma,M.P. (2015) Chromatin fibers are formed by heterogeneous groups of nucleosomes in vivo. *Cell*, **160**, 1145–1158.

59. Ou,H.D., Phan,S., Deerinck,T.J., Thor,A., Ellisman,M.H. and O'Shea,C.C. (2017) ChromEMT: visualizing 3D chromatin structure and compaction in interphase and mitotic cells. *Science*, **357**, eaag0025.

60. Watanabe,S., Kusamaeguchi,K., Kobayashi,H. and Igarashi,K. (1991) Estimation of polyamine binding to macromolecules and Atp in bovine lymphocytes and rat-liver. *J. Biol. Chem.*, **266**, 20803–20809.

61. Igarashi,K. and Kashiwagi,K. (2000) Polyamines: mysterious modulators of cellular functions. *Biochem. Biophys. Res. Commun.*, **271**, 559–564.

62. Makarov,V.L., Lejnine,S., Bedoyan,J. and Langmore,J.P. (1993) Nucleosomal organization of telomere-specific chromatin in rat. *Cell*, **73**, 775–787.

63. McGhee,J.D. and Felsenfeld,G. (1980) Nucleosome structure. *Annu. Rev. Biochem.*, **49**, 1115–1156.

64. Wilson,R.W. and Bloomfield,V.A. (1979) Counter-ion-induced condensation of deoxyribonucleic acid - light-scattering study. *Biochemistry*, **18**, 2192–2196.

65. de Frutos,M., Raspaud,E., Leforestier,A. and Livolant,F. (2001) Aggregation of nucleosomes by divalent cations. *Biophys. J.*, **81**, 1127–1132.

66. Gelbart,W.M., Bruinsma,R.F., Pincus,P.A. and Parsegian,V.A. (2000) DNA-inspired electrostatics. *Phys. Today*, **53**, 38–44.

67. Pegado,L., Jonsson,B. and Wennerstrom,H. (2016) Attractive ion-ion correlation forces and the dielectric approximation. *Adv. Colloid Interface Sci.*, **232**, 1–8.

68. Iwaki,T., Saito,T. and Yoshikawa,K. (2007) How are small ions involved in the compaction of DNA molecules? *Colloids Surf. B*, **56**, 126–133.

69. Arya,G. and Schlick,T. (2009) A tale of tails: how histone tails mediate chromatin compaction in different salt and linker histone environments. *J. Phys. Chem. A*, **113**, 4045–4059.

70. Hansen,J.C. and Lohr,D. (1993) Assembly and structural-properties of subsaturated chromatin arrays. *J. Biol. Chem.*, **268**, 5840–5848.

71. Fletcher,T.M., Serwer,P. and Hansen,J.C. (1994) Quantitative-analysis of macromolecular conformational-changes using agarose-gel electrophoresis - application to chromatin folding. *Biochemistry*, **33**, 10859–10863.

72. Yodh,J.G., Lyubchenko,Y.L., Shlyakhtenko,L.S., Woodbury,N. and Lohr,D. (1999) Evidence for nonrandom behavior in 208–12 subsaturated nucleosomal array populations analyzed by AFM. *Biochemistry*, **38**, 15756–15763.

73. Schwarz,P.M. and Hansen,J.C. (1994) Formation and stability of higher-order chromatin structures - contributions of the histone octamer. *J. Biol. Chem.*, **269**, 16284–16289.

74. Allahverdi,A., Chen,Q., Korolev,N. and Nordenskiold,L. (2015) Chromatin compaction under mixed salt conditions: opposite effects of sodium and potassium ions on nucleosome array folding. *Sci. Rep.*, **5**, 8512.

75. Schwarz,P.M., Felthauser,A., Fletcher,T.M. and Hansen,J.C. (1996) Reversible oligonucleosome self-association: dependence on divalent cations and core histone tail domains. *Biochemistry*, **35**, 4009–4015.

76. Maeshima,K., Rogge,R., Tamura,S., Joti,Y., Hikima,T., Szerlong,H., Krause,C., Herman,J., Seidel,E., DeLuca,J. *et al.* (2016) Nucleosomal arrays self-assemble into supramolecular globular structures lacking 30-nm fibers. *EMBO J.*, **35**, 1115–1132.

77. Post,C.B. and Zimm,B.H. (1982) Theory of DNA condensation - collapse versus aggregation. *Biopolymers*, **21**, 2123–2137.

78. Post,C.B. and Zimm,B.H. (1982) Light-scattering study of DNA condensation - competition between collapse and aggregation. *Biopolymers*, **21**, 2139–2160.

79. Post,C.B. and Zimm,B.H. (1980) DNA condensation and how it relates to phase-equilibrium in solution. *Biophys. J.*, **32**, 448–450.

80. Finch,J.T. and Klug,A. (1976) Solenoidal model for superstructure in chromatin. *PNAS*, **73**, 1897–1901.

81. Maeshima,K., Ide,S., Hibino,K. and Sasai,M. (2016) Liquid-like behavior of chromatin. *Curr. Opin. Genet. Dev.*, **37**, 36–45.

82. Noguchi,H. and Yoshikawa,K. (1998) Morphological variation in a collapsed single homopolymer chain. *J. Chem. Phys.*, **109**, 5070–5077.

83. Smith,S.B., Finzi,L. and Bustamante,C. (1992) Direct mechanical measurements of the elasticity of single DNA-molecules by using magnetic beads. *Science*, **258**, 1122–1126.

84. Hajjoul,H., Mathon,J., Ranchon,H., Goiffon,I., Mozziconacci,J., Albert,B., Carrivain,P., Victor,J.M., Gadal,O., Bystricky,K. *et al.* (2013) High-throughput chromatin motion tracking in living yeast reveals the flexibility of the fiber throughout the genome. *Genome Res.*, **23**, 1829–1838.

85. Cui,Y. and Bustamante,C. (2000) Pulling a single chromatin fiber reveals the forces that maintain its higher-order structure. *PNAS*, **97**, 127–132.

86. Yoshikawa,K. and Matsuzawa,Y. (1996) Nucleation and growth in single DNA molecules. *J. Am. Chem. Soc.*, **118**, 929–930.

87. Vilfan,I.D., Conwell,C.C., Sarkar,T. and Hud,N.V. (2006) Time study of DNA condensate morphology: implications regarding the nucleation, growth, and equilibrium populations of toroids and rods. *Biochemistry*, **45**, 8174–8183.

88. Conwell,C.C. and Hud,N.V. (2004) Evidence that both kinetic and thermodynamic factors govern DNA toroid dimensions: Effects of magnesium(II) on DNA condensation by hexammine cobalt(III). *Biochemistry*, **43**, 5380–5387.

89. van den Broek,B., Noom,M.C., van Mameren,J., Battle,C., MacKintosh,F.C. and Wuite,G.J.L. (2010) Visualizing the formation and collapse of DNA toroids. *Biophys. J.*, **98**, 1902–1910.

90. Hud,N.V. (1995) Double-stranded DNA organization in bacteriophage heads - an alternative toroid-based model. *Biophys. J.*, **69**, 1355–1362.

91. Yamada,A., Kubo,K., Nakai,T., Yoshikawa,K. and Tsumoto,K. (2005) All-or-none switching of transcriptional activity on single DNA molecules caused by a discrete conformational transition. *Appl. Phys. Lett.*, **86**, 223901.

92. Yodh,J.G., Woodbury,N., Shlyakhtenko,L.S., Lyubchenko,Y.L. and Lohr,D. (2002) Mapping nucleosome locations on the 208–12 by AFM provides clear evidence for cooperativity in array occupation. *Biochemistry*, **41**, 3565–3574.